12th AIAA Aviation Technology, Integration, and Operations (ATIO) Conference and 14th AIAA/ISSM
17 - 19 September 2012, Indianapolis, Indiana

AIAA 2012-5629

Large Scale Aeroelastic Data for Design of Rotating Blades using Navier-Stokes Equations

Guru P. Guruswamy *
NASA Advanced Supercomputing Division
Ames Research Center, Moffett Field, CA

Abstract

Bending-torsion flutter boundaries for rotating blades are computed using unsteady aerodynamic data obtained by time accurately solving the Navier-Stokes equations. A modal approach is used for computing the flutter boundary. Flutter speeds are computed by solving eigenvalue equations that track down the system damping to identify flutter point. Aerodynamic data required for the analysis is computed by time accurately integrating aerodynamic equations while the blades are undergoing modal motions at various oscillating frequencies. Validity of the approach is established by comparing the flutter speed results with those measured for a non-rotating blade. Results are demonstrated for a typical rotating blade. Parallel computing resources are utilized to cope with computational costs associated with use of the Navier-Stokes equations.

Nomenclature

c	=	chord length
C_l, C_m	=	sectional lift and moment coefficients
{d}	=	displacements
{f}, {F}	=	actual and modal aerodynamic force vectors
g	=	structural damping coefficient
h	=	generalized displacements
k	=	reduced frequency, $\omega c/U$
M	=	Mach number
q	=	dynamic pressures, $0.5\rho U^2$
R, r	=	blade span, distance from root
[s], [S]	=	actual and modal stiffness matrices
U, U_f	=	blade speed of a given section, varying and at flutter
[w],[W]	=	actual and modal mass matrix
t	=	time in seconds
ρ	=	air density
$\omega, \omega_f, \omega_h, \omega_\alpha$	=	general, flutter, bending, torsional frequencies in rad/sec
Ω	=	rotating speed in radians per second
[Φ]	=	mode shape matrix
λ	=	flutter Eigen value
∞	=	represents free stream condition
η	=	air to mass density ratio

I Introduction

The evaluation of flutter characteristics of rotor blades is critical to avoid structural failures [1]. Flows over rotating blades are often dominated by complexities such as blade-vortex interactions and moving shock waves [2]. Wind tunnel experiments in this area are rare due to the high expenses involved, and flight tests are almost impossible due to high risk [3]. As a result, computational procedures have become essential to address the dynamic aeroelastic problems of rotating blades.

---

* Sr. Scientist, Applied Modeling and Simulation Branch, AIAA Associate Fellow

Currently, computational methods based on linear aerodynamic codes are in routine use for computing the aeroelastic characteristics of rotating blades [4]. However, methods based on the Navier-Stokes flow equations are needed to model flow complexities such as blade-vortex interactions and moving shock waves that cannot be modeled using the linear aerodynamic equations of motion.

The calculation of aeroelastic responses using computational fluid dynamics (CFD) and computational structural dynamics (CSD) methods began with the development of the Transonic Small Perturbation (TSP) theory [5]. An original approach to compute flutter boundaries based on CFD-TSP, using both coupled (time-domain) and uncoupled (frequency-domain) CFD/CSD methods with cross validations, is presented in Ref. [6]. These methods were extended to 3D cases, in the frequency domain (i.e., uncoupled) using TSP [7] and the time domain (i.e., coupled) using the Euler equations [8]. Such CFD based time-domain aeroelastic method developed in early 90's [8] is successfully applied for flutter boundary identification [9].

The process of generating aeroelastic loads for rotating blades by correcting the look-up table-based airloads using loads from the Navier-Stokes equations is in routine use [10]. This procedure, which uses beam finite elements for structural deflections, is also called the loose coupling approach. Recently, Euler/Navier-Stokes based time-accurate aeroelastic computations for helicopter blades have been computed. Reference [11] presents an application for an isolated, single blade using a time integration approach similar to that shown for fixed wings [8]. This time response approach is computationally more expensive than the frequency response approach for computing flutter boundaries, as responses need to be computed for changes in every design parameter.

Several parameters, such as advance ratio, angle of attack, rotating speed and structural properties, need to be considered for the design. Under certain assumptions, a good prediction of a flutter boundary can be made using the frequency domain (uncoupled approach) [6]. The primary assumption in the frequency domain approach is that the aerodynamic loads can be linearly superimposed among modes, and because flutter starts as a small perturbation phenomenon. This approach has served as a valid tool for computing flutter boundaries [7].

This paper describes a method for computing the bending-torsion flutter boundaries for rotating blades, using the frequency domain approach. The unsteady, aerodynamic data is obtained by time accurately solving the Navier-Stokes equations while the blade is undergoing oscillatory rotations. A modal approach is then used to compute the flutter boundary. Flutter speeds are computed using an Eigenvalue approach that tracks down system damping to identify flutter [12]. Aerodynamic data required for the analysis is computed by time accurately integrating the aerodynamic equations while the blade is undergoing modal motions at various oscillating frequencies. Validity of the approach is established by comparing the flutter speed results with those measured for the non-rotating blades. Results are demonstrated for a typical rotating blade. Parallel computing resources are utilized to cope with computational costs associated with use of the Navier-Stokes equations.

II Approach

Following the finite element formulation, Lagrange's equation of motion is defined as:

$$[w]\{\ddot{d}\}+[s]\{d\}=\{f\} \qquad (1)$$

where [w], and [s] are the mass and stiffness matrices, respectively, and {d} and {f} are the displacement and force vectors.

Based on Raleigh-Ritz method the governing aeroelastic Eq. (1) can be re-formulated using modes. In this approach aeroelastic displacements at any time are expressed as functions of a finite set of modes using:

$$\{d\}=[\Phi]\{h\} \qquad (2)$$

where $[\Phi]$ is the modal shape matrix and {h} is the generalized displacement vector.

Applying (2) to (1) yields:

$$[W]\{\ddot{h}\}+[S]\{h\}=\{F\} \tag{3}$$

where modal mass is $[W]=[\Phi]^T\{w\}[\Phi]$ (4a)

and modal stiffness is $[S]=[\Phi]^T\{s\}[\Phi]$ (4b)

The modal force vector is obtained by perturbing the structures, which results in:

$$\{F\}=[\Phi]^T\{f\} \tag{5a}$$
$$\{F\}=q[\Phi]^T[P]\{d\} \tag{5b}$$
$$\{F\}=q[\Phi]^T[P][\Phi]\{h\} \tag{5c}$$

where q is the dynamic pressure, defined as $q=1/2\rho U^2$, ρ is the free stream air density, and U is the speed of the blade. The diagonal force coefficient matrix [P] is the integrated airloads over blade span due to perturbing the blade by the modal displacements. Thus, the generalized aerodynamic force Q_{ij} is written as:

$$Q_{ij}=q\{\Phi_i\}^T[P]\{\Phi_j\} \tag{6}$$

Q_{ij} represents the modal force acting in the ith mode caused by pressure generated by the modal motion of jth mode. Since the blade speed varies along the radius values at 75 percent span station are selected for reference [13].

A flutter boundary is computed by using the U-g (velocity-damping) method [12]. The U-g method uses the fact that the flutter starts as a harmonic motion with small amplitude, so that the generalized displacements {h} take the form:

$$\{h\}=\{\bar{h}\}e^{i\omega t} \tag{7}$$

where ω is the circular frequency at flutter. Following the procedure in Ref. [12], structural damping, g, is introduced by replacing ωwith complex value ω(1+ig).

For both fixed wings and rotor blades, a bending-torsion flutter boundary determines structural integrity. Bending-torsion flutter can occur for rotating blades with low torsional stiffness, as well as for cases such as transonic flow where the center of pressure is away from the elastic axis [14].

In the design phase, it is important to assure the safety of a blade by knowing its bending-torsion flutter boundary. In this work, Eq. (2) is modified to compute the bending-torsion flutter of rotating blades. As suggested in Ref. [13], the 75 percent radial station is considered as a reference section to compute the flutter boundary. The reduced frequency k_r is defined as $4\omega_f c/3\Omega R$, where ω_f is the oscillatory flutter frequency, c is the chord length, Ω is the rotating speed in radians per second, and R is the blade radius. Equation (2) can be rewritten as:

$$\eta k_r^2 \left[[\bar{W}] - [A] \right] \begin{Bmatrix} \bar{h}_1 \\ \bar{h}_2 \end{Bmatrix} = \lambda [\bar{S}] \begin{Bmatrix} \bar{h}_1 \\ \bar{h}_2 \end{Bmatrix} \tag{8}$$

where $\bar{h}_1$ and $\bar{h}_2$ are generalized displacements corresponding to bending and torsional modes, respectively. Also defined are the air-to mass density ratio [13] $\eta = W_{11}/(\pi \rho R c^2)$ and

$$\left[\bar{W} \right] = \begin{bmatrix} 1 & e \\ e & \gamma^2 \end{bmatrix} \tag{9}$$

where $\gamma^2 = 2\bar{W}_{12}/(W_{11}c)$ and $e = 4\bar{W}_{22}/(W_{11}c^2)$.

Since the blades have large aspect ratios, the assumed bending mode and torsion modes [13] are defined as $\Phi_1 = (r/R)^2$ and $\Phi_2 = (r/R)$, respectively, where r is the distance from the blade rotating axis. Then, elements of the aerodynamic matrix [A] can be defined by

$$A_{11} = \int_0^R Q_{11} \Phi_1^2 \delta r$$

$$A_{12} = \int_0^R Q_{12} \Phi_1 \Phi_2 \delta r$$

$$A_{21} = \int_0^R Q_{21} \Phi_2 \Phi_1 \delta r$$

$$A_{22} = \int_0^R Q_{22} \Phi_2^2 \delta r$$

Assuming ω_h and ω_α are bending and torsion oscillatory frequencies, yields

$$[\bar{S}] = \begin{bmatrix} (\omega_h/\omega_f)^2 & 0 \\ 0 & \gamma^2 (\omega_\alpha/\omega_f)^2 \end{bmatrix} \tag{10}$$

The eigenvalue λ in Eq. (8) is defined as:

$$\lambda = \eta(1+ig)\omega_f^2 c^2 / 4U^2 \tag{11}$$

The eigenvalue λ in Eq. (8) is solved to compute the non-dimensional flutter speed: $\bar{U} = 2U/c\omega_\alpha$ and flutter reduced frequency $k_f = 4\omega_f c/3\Omega R$.

For a given rotating speed the U-g approach needs aerodynamic forces at various oscillatory-reduced frequencies for selected modes. Oscillatory frequencies are varied while the blade is rotating at a given speed Ω. Once the airloads are computed for two modes in the form of real and imaginary values at various frequencies, the complex eigenvalue in Eq. (8), is solved. Flutter speed is determined when the damping changes from a positive to a negative value. These computations are repeated for different rotating speeds.

Airloads are computed by solving the Navier-Stokes equations using the diagonal form of the Beam-Warming implicit finite difference method [15], available in the latest version of NASA's the OVERFLOW code [16] that utilizes the Spalart-Allmars turbulence model. This version is suitable for flexible rotating blades.

III Solution Procedure on Parallel Computers

The computation of flutter boundaries needs unsteady airloads from CFD at different rotating speeds, oscillatory frequencies, and mode shapes. Unsteady airload computations using the Navier-Stokes equations for multiple cases need large amounts of computer time. The computational resources issue can be alleviated by using parallel computers. The present computational scenario is ideal for massively parallel computations. In the work described here, computations are made on NASA's Pleiades supercomputer with the Linux operating system-based MPIexec utility [17]. MPIexec runs multiple cases in parallel within a single job environment. Therefore, the wall-clock time for multiple cases will be essentially equal to that for a single case [17] if adequate processors are utilized.

The mode shapes are generated for bending and torsion modes for various frequencies. Input for the CFD is generated for different rotating speeds. Airloads are computed in parallel for various rotating speed, mode shape, and modal frequency. Real and imaginary values of unsteady airloads are computed using Fourier analysis. These airloads are used as input to the eigenvalue flutter solution module, MODFLU, which solves Eq. (8). Since many steps are involved in computing the flutter speed, the procedure is streamlined within an Unix script, RUNMOD, similar to the RUNPBS script presented in Ref. [17].

IV Results

A. Validation for Non-Rotating Blades

The method developed here is first validated for non-rotating simple rectangular blades that have measured unsteady loads and flutter boundary data. Flow computations are made using a single C-H grid with 250K grid points. This type of grid topology that has a moderate grid size yields satisfactory unsteady results for simple rectangular wings [11]. Correct prediction of flutter speed requires accurate unsteady airloads. The accuracy of the finite difference solver used for flow solutions is validated by computing airloads for a flapping blade with a 6 percent circular arc [18]. Figure 1 shows the comparison of the magnitude and phase angles of unsteady lifting pressures with wind tunnel test data at a 70 percent radial station. The 70% station is selected for comparison since it is the station closest to the 75% station typically recommended [13] for comparison flutter characteristics between of rotating and non-rotating wings. The blade is flapping with a reduced frequency k, (defined as $\omega c/U$) = 0.26 and M_∞ = 0.90. Computed results show good comparison with measured data.

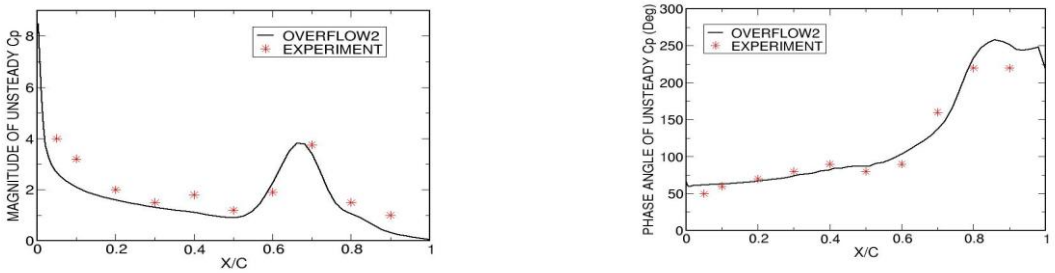

(a) (b)

Fig. 1 Validation of magnitude (a) and phase angles (b) of unsteady pressures at 70% span for a flapping blade, Ref. 18.

Computation of flutter boundary using the RUNMOD script is validated for a non-rotating blade that has wind tunnel flutter-boundary data [19] for a blade with an aspect ratio of 5 and a parabolic arc with a thickness of 6 percent. Flutter speeds are computed for ten Mach numbers ranging from 0.7 to 1.2 using five frequencies of flapping and torsional modes. The airloads for 100 cases are obtained in a single run using the MPIexec utility in RUNMOD. The total wall-clock time is about 30 minutes using 100

processors. Figure 2 shows a plot of speed ($U/b\omega_\alpha$) vs. structural damping for both modes at $M_\infty = 0.80$. Flutter occurs when damping g of mode 1 changes from positive to negative.

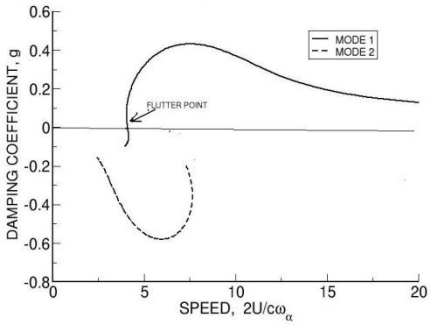

Fig. 2 Plot of scaled speed vs system damping coefficient at Mach 0.8.

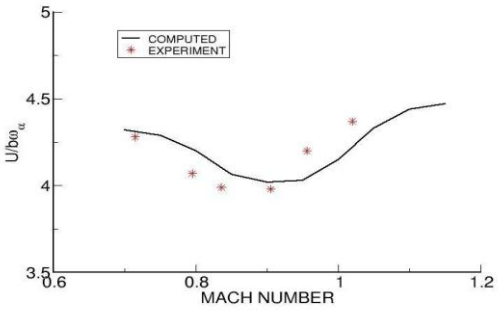

Fig. 3 Validation of flutter boundary of a non-rotating blade, Ref. 19.

Figure 3 shows a comparison of flutter speed ($U_f/b\omega_\alpha$) between the computed and measured data. Both agree in trend and values. The flutter speed decreases with the increase in Mach number until about Mach 0.95, and then it starts rising as the Mach number reaches supersonic speed. The computed flutter speeds are higher than that measured until about Mach 0.97 then it is lower. Flutter speed appears to flatten out at low subsonic and high supersonic Mach numbers.

Results in figures 1 and 3 show that the RUNMOD procedure using the Navier-Stokes data and the eigenvalue flutter speed solver of Eq. (8) are verified for non-rotating blades. The remainder of the paper demonstrates results for a typical rotating blade.

B. Rotating Blade Results

1. CFD Grid

All computations are made for a rectangular blade that has an aspect ratio of 10, with a NACA0012 airfoil section. The blade is modeled using the C-O grid with cap grids for the tip and root. The near-body grids for the blade, root, and tip have 1000K, 260K, and 150K grid points, respectively. The normal grid spacing on the blade surface is about $8x10^{-5}$ of the chord. The total grid, including the outer grids, is about 1800K points. The outer grid boundaries are located at about 10 times the radius R of the blade. This topology is based on the grid that was successfully used to validate a rotor system configuration [16]. A portion of the grid near the tip is shown in Fig. 4.

The mode shape data is generated using assumed modes for bending and torsional modes. The ratio of bending frequency to torsional frequency is set to 0.3, a typical value for rotor blades. The mass center is at 45 % chord length, and the elastic axis is at 0.25 % chord. The oscillating frequency ω of the blade is varied as a percentage of rotating frequency Ω. A plot of the tip motions for various frequency ratios with respect to azimuth are shown in Fig. 5 for the twisting mode. Using these mode shapes for flapping and bending modes, prescribed motion files for the CFD code are generated [16]. The collective angle is set to10 degrees and tip amplitudes are set to 1 degree. For bending modes, tip amplitudes are set to 0.05 percent of the blade span.

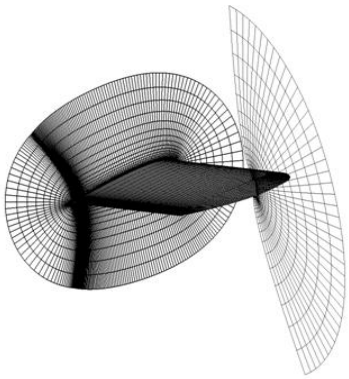

Fig. 4 Portion of the grid near the tip.

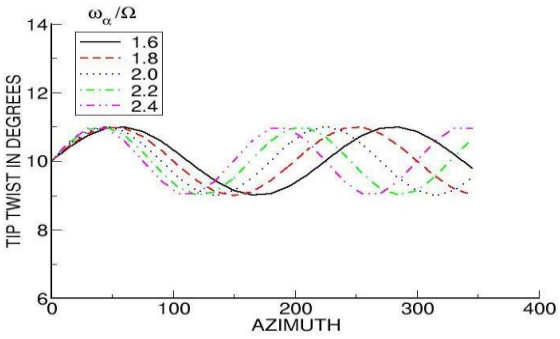

Fig. 5 Twist mode shapes for rotating blade.

2. Time Step Convergence

Time step convergence is established based on the rotating speed. The blade is rotated in increments of 720 steps per revolution (NSPR), starting from NSPR = 720. It is oscillated in its first torsional mode with a frequency twice the rotational frequency, i.e., $\omega = 2\Omega$. Figure 6 shows plots of average sectional loads with respect to radius. Spanwise loads converge at NSPR = 3600. The rest of the computations are made using NSPR = 3600.

3. Flutter Boundary Computations

Flutter speeds are computed for 10 rotating speeds, from Ω= 55 to 100, in increments of five for two types of mode at five oscillating frequencies. The oscillatory frequencies are 1.6, 1.8, 2.0, 2.2, and 2.4 times the rotating frequencies. This leads to computing unsteady airloads for 100 cases. Each case requires about 23 hours of CPU time on a single node of the Pleiades supercomputer [17]. Using MPIExec, all cases run in parallel within about 24 hours, using 100 Pleiades nodes.

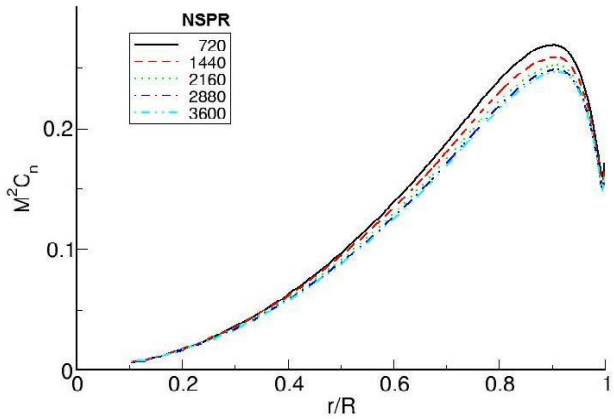

Fig. 6 Average sectional lifts for increasing NSPR.

Figure 7 shows plots of flutter speed vs. rotating speed. Flutter speeds are also shown for the rotating blade without accounting for change in the stiffness due to centrifugal force. The differences are more pronounced for higher rotating speeds, as expected. Flutter boundaries are also compared with an equivalent fixed blade using the flow characteristics at 75 % radial station. The flutter boundary for the fixed blade is lower than that for rotating blade including the effect of centrifugal force. This may be attributed to lower stiffness due to the absence of added centrifugal stiffness in non-rotating blade. The corresponding results for flutter frequency are shown in Fig. 8. The centrifugal force has less influence on frequency than on flutter speed, and the effect appears to be on the same order for all rotating speeds considered. The flutter frequency for the fixed blade is higher than rotating blade up to about $\Omega = 75$ then it is lower.

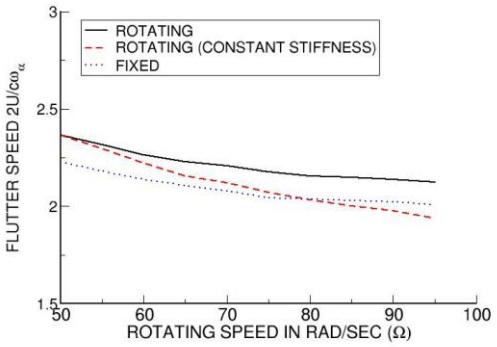

Fig. 7 Flutter boundary speed vs. rotating speeds.

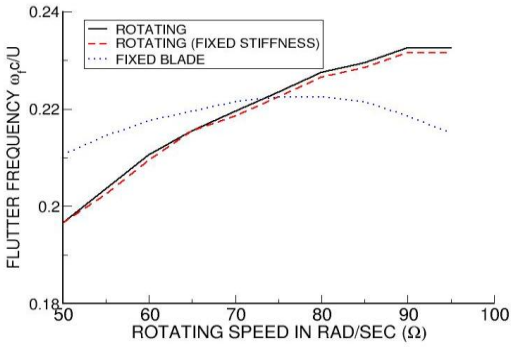

Fig. 8 Flutter frequency plots.

V Conclusions

A procedure to compute the bending-torsion flutter boundaries of rotating blades using unsteady loads from the Navier-Stokes flow equations is presented. A frequency-domain mathematical formulation that results in eigenvalue equations based on airloads obtained by from a Navier-Stokes solver is formulated. Large computational requirement associated with the use of high-fidelity Navier-Stokes equations is addressed using parallel computers. Unsteady airloads and flutter speeds for non-rotating blades predicted compare well with measured data. Results demonstrated for a typical rotating blade establishes the practical use of the procedures developed. Equations formulated are suitable for adding additional degrees-of-freedom such as lead-lag motion.

References

1. Mil' M. L., "Helicopters Calculation and Design-Volume I: Aerodynamics," NASA TT F-494, Sept. 1967, pp. 379-380.

2. Meakin, R., "Unsteady Simulation of the Viscous Flow about a V-22 Rotor and Wing in Hover," AIAA-95-3463-CP, AIAA Atmospheric Flight Mechanics Conference, Baltimore, MD, August 1995.

3. Lind, R. and Brenner, M., "Robust Flutter Margins of an F/A-18 Aircraft from Aeroelastic Flight Data," *J. of Guidance and Control, and Dynamics*, Vol. 20, No. 3, May-June 1997, pp. 597-604.

4. "RCAS Theory Manual, Version 2.0," USAMCOM/AFDD TR 02-A-005, US Army Aviation and Missile Command, Moffett Field, CA, June 2000.

5. Ballhaus, W. F. and Bridgeman, J. O., "Numerical Solution Techniques for Unsteady Transonic problems," AGARD Rep No 679, Paper No.16 (1980).

6. Guruswamy, P. and Yang, T.Y., "Aeroelastic Time Response of Thin Airfoils," *International J. of Computers and Fluids*, Vol. 9, No. 4, 1981, pp. 409-425.

7. Guruswamy, G. P. and Goorjian, P. M., "Computations and Aeroelastic Applications of Unsteady Transonic Aerodynamics About Wings," *J. of Aircraft*, Vol. 21, No. 1, Jan. 1984, pp. 37-43.

8 Guruswamy, G. P. "Unsteady Aerodynamic and Aeroelastic Calculations for Wings Using Euler Equations," *AIAA J.*, Vol. 28, No. 3, March 1990, pp. 461-469, (also AIAA Paper 88-2281).

9. McNamara, J. J, and Friedmann, P. P., "Flutter-Boundary Identification for Time-Domain Computational Aeroelasticity," AIAA J., Vol. 45, No 7, July 2007, pp 1546-1555.

10. Datta, A. and Chopra, I., "Validation and Understanding of UH-60A Vibratory Loads in Steady Level Flight," *J. of the American Helicopter Society*, Vol. 49, (3), July 2004, pp. 271-287.

11. Guruswamy, G.P., "Computational-Fluid-Dynamics and Computational-Structural-Dynamics Based Time-Accurate Aeroelasticity of Helicopter Blades," *J. of Aircraft*, Vol. 47, No. 3, May-June 2010, pp. 858-863.

13. Fung, Y.C, "Fundamentals of Flutter Analysis," *An Introduction to the Theory of Aeroelasticity*, Dover Publication Inc., New York, Nov. 1968, pp. 186-245.

13. Bielava, R. L., "Unsteady Aerodynamics and Flutter," *Rotary Wing Structural Dynamics and Aeroelasticity*, AIAA Education Series, Washington D.C., 1992, pp. 379-454.

14. Dowell, E., "Aeroelastic Response of Rotorcraft," *A Modern Course in Aeroelasticity*, Kluwer academic Publishers, The Netherlands, 2004, pp. 377-481.

15. Beam, R. M. and Warming, R. F, "An Implicit Factored Scheme for the Compressible Navier-Stokes Equations," *AIAA J.*, Vol.16, No 4, 1978, pp. 393-402.

16. Boyd, D. D., "HART-II Acoustic Predictions using a Coupled CFD/CSD methods," American Helicopter Society 65th Annual Forum, Grapevine Texas, May 2009.

17. Guruswamy, G. P., "Large-Scale Computations for Stability Analysis of Launch Vehicles Using Cluster Computers," *J. of Spacecraft and Rockets*, Vol. 48, No. 4, 2011, pp. 584-588.

18. Lessing, H. C., Troutman, J. L., and Menees, G. P., "Experimental Determination of the Pressure Distribution on a Rectangular Wing Oscillating in the First Bending Mode for Mach Numbers 0.24 to 1.30," NASA TN D-344, Dec. 1960.

19. Dogget, R. V., Rainey, A. G, and Morgan, H. G, "An Experimental Investigation on Transonic Flutter Characteristics," NASA TMX-79, Nov. 1959.